



**HAL**  
open science

## **Interplay between myofibers and pro-inflammatory macrophages controls muscle damage in mdx mice**

Marielle Saclier, Sabrina Ben Larbi, Ha My Ly, Eugénie Moulin, Rémi Mounier, Bénédicte Chazaud, Gaëtan Juban, Sabrina Ben Larbi, Ha My Ly

### ► **To cite this version:**

Marielle Saclier, Sabrina Ben Larbi, Ha My Ly, Eugénie Moulin, Rémi Mounier, et al.. Interplay between myofibers and pro-inflammatory macrophages controls muscle damage in mdx mice. *Journal of Cell Science*, 2021, 134 (18), pp.jcs258429. 10.1242/jcs.258429 . inserm-03404658

**HAL Id: inserm-03404658**

**<https://inserm.hal.science/inserm-03404658>**

Submitted on 26 Oct 2021

**HAL** is a multi-disciplinary open access archive for the deposit and dissemination of scientific research documents, whether they are published or not. The documents may come from teaching and research institutions in France or abroad, or from public or private research centers.

L'archive ouverte pluridisciplinaire **HAL**, est destinée au dépôt et à la diffusion de documents scientifiques de niveau recherche, publiés ou non, émanant des établissements d'enseignement et de recherche français ou étrangers, des laboratoires publics ou privés.

**Myofiber / pro-inflammatory macrophage interplay controls muscle damage in mdx mice**

Marielle Saclier<sup>1</sup>, Sabrina Ben Larbi<sup>2</sup>, Ha My Ly<sup>2</sup>, Eugénie Moulin<sup>2</sup>, Rémi Mounier<sup>2</sup>, Bénédicte Chazaud<sup>2</sup>, Gaëtan Juban<sup>2</sup>

1- Department of Biosciences, University of Milan, 20133 Milan, Italy

2- Institut NeuroMyoGène, Université Claude Bernard Lyon 1, CNRS UMR 5310, INSERM U1217, Université de Lyon, Lyon, France

Corresponding author:

Gaëtan Juban

Institut NeuroMyoGène,

8 Avenue Rockefeller

69008 Lyon, France

Tel: (33) 4 26 68 82 49

[gaetan.juban@univ-lyon1.fr](mailto:gaetan.juban@univ-lyon1.fr)

**KEYWORDS**

Duchenne muscular dystrophy – macrophage – fibrosis – myofiber branching - AMPK

## **Summary**

Duchenne Muscular Dystrophy is a genetic muscle disease characterized by chronic inflammation and fibrosis, mediated by a pro-fibrotic macrophage population expressing pro-inflammatory markers. Our aim was to characterize cellular events leading to the alteration of macrophage properties, and to modulate macrophage inflammatory status using the gaseous mediator H<sub>2</sub>S. Using co-culture experiments, we first showed that myofibers derived from mdx mice strongly skewed the polarization of resting macrophages towards a pro-inflammatory phenotype. Treatment of mdx mice with NaHS, an H<sub>2</sub>S donor, reduced the number of pro-inflammatory macrophages in skeletal muscle, which was associated with a decreased number of nuclei per fiber, together with a reduced myofiber branching and fibrosis. Finally, we established the metabolic sensor AMPK as a critical NaHS target in muscle macrophages. These results identify an interplay between myofibers and macrophages where dystrophic myofibers contribute to the maintenance of a highly inflammatory environment sustaining a pro-inflammatory macrophage status, in turn favoring myofiber damage, myofiber branching and fibrosis establishment. They also identify H<sub>2</sub>S donors as a potential therapeutic strategy to improve dystrophic muscle phenotype by dampening chronic inflammation.

## **Introduction**

Adult skeletal muscle completely regenerates after an injury, thanks to the muscle stem cells (MuSCs) or satellite cells, that sustain adult myogenesis. This includes activation, proliferation, commitment into terminal myogenesis, differentiation and fusion to form new myofibers. The regeneration power of adult skeletal muscle is very high and damaged muscle fully recovers its functions within a few weeks. While MuSCs are absolutely indispensable for skeletal muscle regeneration, surrounding cells also play important roles in this process, including endothelial cells, fibro/adipogenic progenitors (FAPs) and immune cells (Bentzinger et al., 2013).

Particularly, macrophages are crucial for efficient muscle regeneration. As in other damaged tissues, the first macrophages to invade the injured area are pro-inflammatory damage-associated macrophages that mainly arise from circulating monocytes. Inflammatory damage-associated macrophages express pro-inflammatory effectors that stimulate MuSC proliferation (Saclier et al., 2013), while limiting FAP expansion (Juban et al., 2018; Lemos et al., 2015). Phagocytosis of debris participates to the resolution of inflammation, which is crucial to start tissue repair and regeneration (Arnold et al., 2007). Resolution of inflammation is characterized by a progressive switch of the inflammatory profile exhibited by macrophages, that become anti-inflammatory or recovery macrophages. This process is controlled by several molecular effectors, including the metabolic sensor AMPK (Mounier et al., 2013), the IGF1 pathway (Tonkin et al., 2016), the p38 regulator MKP-1 (Perdiguero et al., 2014), and the transcription factors C/EBP $\beta$  (Ruffell et al., 2009) and NFIX (Saclier et al., 2020). These anti-inflammatory macrophages exert a variety of effects on surrounding cells: they stimulate the last steps of myogenesis, including differentiation and fusion (Saclier et al., 2013), they activate FAPs to remodel the extracellular matrix (ECM) (Juban et al., 2018; Lemos et al., 2015), and favor angiogenesis, which occurs concomitantly to myogenesis (Latroche et al., 2017).

Post-acute injury skeletal muscle regeneration is a highly regulated process, during which the various stages described above must be well coordinated in space and time. The situation is drastically different in degenerating myopathies, such as Duchenne Muscular Dystrophy

(DMD), during which multiple injuries occur asynchronously throughout the muscle. Skeletal muscle in degenerative myopathies fails to regenerate because of these permanent and asynchronous cycles of degeneration-regeneration due to mutations in the dystrophin-glycoprotein complex, which ensures myofiber integrity (Lapidos et al., 2004). In these disorders, recurrent myofiber damage leads to chronic inflammation and the eventual establishment of fibrosis. Indeed, it was shown that asynchronous injuries in normal muscle trigger a chronic inflammatory status in the muscle associated with a fibrotic signature, reminiscent of what is observed in degenerative myopathies (Dadgar et al., 2014).

Macrophages are associated with fibrosis in mdx muscle, the mouse model for DMD (Vidal et al., 2008). Inhibition of the pro-inflammatory NF- $\kappa$ B pathway is associated with a lower macrophage number and a better phenotype of the muscle (Acharyya et al., 2007). Similarly, preventing the entry of circulating monocytes into the muscle temporarily improves muscle histology and function (Liang et al., 2018; Mojumdar et al., 2014; Wehling et al., 2001). However this is detrimental on a longer term (Zhao et al., 2016), showing the pivotal role of macrophages during muscle regeneration, and the necessity to target the right subset to prevent disease progression. Recently, we showed in an experimentally fibrotic mdx mouse model, that fibrosis is associated with pro-inflammatory macrophages (Juban et al., 2018). Functionally, these macrophages stimulate matrix production by fibroblastic cells through the abnormal secretion of latent TGF $\beta$ , due to an increased expression of the gene encoding a Latent TGF-beta binding protein (LTBP), that is involved in latent TGF $\beta$  export into the ECM. Interestingly, pharmacological skewing of these macrophages towards an anti-inflammatory phenotype using an AMPK activator improves muscle phenotype and function (Juban et al., 2018).

The standard treatment for DMD patients consists of Glucocorticoids (GCs), which have been shown to delay disease progression and ambulation loss (McDonald et al., 2018). However, chronic daily exposure to GCs is associated with adverse effects including obesity, metabolic changes and muscle atrophy (Schakman et al., 2013; Wood et al., 2015). Therefore, alternative therapeutic strategies are required. Hydrogen Sulfide (H<sub>2</sub>S) is an endogenously

synthesized small gaseous signaling molecule that is freely permeable to cell membrane (Wang, 2014). H<sub>2</sub>S is involved in various biological processes, including inflammation. Alteration of H<sub>2</sub>S levels have been associated with several diseases in human or animal models, including sepsis, diabetes or rheumatoid arthritis (Fagone et al., 2018). H<sub>2</sub>S has emerged as a promoter of the resolution of inflammation through the regulation of macrophage inflammatory state (Sun et al., 2020; Wallace et al., 2012). Interestingly, H<sub>2</sub>S-releasing molecules, like NaHS, have been shown to reduce skeletal muscle atrophy in a mouse model of diabetes (Lu et al., 2020) and to decrease muscle fibrosis after contusion-induced injury (Zhao et al., 2020). Moreover, H<sub>2</sub>S-releasing molecules have shown promising results in cardiovascular disorders and arthritis with reduced adverse effects (Wallace et al., 2020; Wallace et al., 2018).

In the present study, we investigated the interaction between myofibers and macrophages in the context of degenerative myopathies. As the macrophage phenotype is modulated by their close environment, we tested the hypothesis that dystrophic muscle fibers may themselves alter macrophage status, using *ex vivo* coculture experiments. Then, we analyzed the possibility to modulate the macrophage phenotype *in vivo* using NaHS, an H<sub>2</sub>S donor, to ameliorate dystrophic muscle phenotype. Finally, we identified the metabolic sensor AMPK as an essential NaHS mediator in macrophages.

## **Results**

### **DMD-derived myofibers trigger pro-inflammatory profile of macrophages**

The role of myofibers on macrophage polarization was investigated by coculturing wild-type bone marrow derived macrophages (BMDMs) with single fibers isolated from wild-type and dystrophic muscle (Fig.1A). Wild-type myofibers increased the expression of 2 out of 4 pro-inflammatory markers analyzed by resting macrophages (Fig.1B-C, +23% for TNF $\alpha$  and +37% for COX2 as compared with control). However, in the presence of mdx myofibers, the number of BMDMs expressing pro-inflammatory markers was strongly increased: it increased the expression of 3 out of 4 pro-inflammatory markers: TNF $\alpha$ , CCR2 and COX2 (Fig.1B-C, 45, 30

and 58% increase as compared with control, respectively). Importantly, this was not associated with a difference in mortality between wild-type and mdx myofibers after 3 days of culture (Fig.S1). No modification of the expression of the anti-inflammatory markers CD301 and ARG1 by BMDMs was observed when cocultured with wild-type or mdx myofibers (Fig.1B-C). These results show that mdx myofibers skew macrophages towards a pro-inflammatory phenotype. Thus, not only the cycles of injury/regeneration, but also the dystrophic myofibers themselves sustain the inflammation in mdx muscles, highlighting the relevance of modulating inflammation as a therapeutic strategy.

### **NaHS treatment reduces pro-inflammatory macrophages in dystrophic muscle**

In an attempt to modulate the macrophage inflammatory status, we treated 3-month-old mdx mice with NaHS, an H<sub>2</sub>S donor. Because of the short half-life of H<sub>2</sub>S *in vivo* (Calvert et al., 2010), NaHS was delivered intraperitoneally daily for 3 weeks (Fig.2A). NaHS treatment induced an important decrease in the number of macrophages per myofiber in the *Tibialis Anterior* (TA) muscle (Fig.2B, -42%) and in the diaphragm (Fig.2C, -56%). More precisely, in TA from NaHS treated mice, a strong decrease in the number of macrophages expressing pro-inflammatory markers was observed (Fig.2D-E, -35 and -31% for TNF $\alpha$  and iNOS, respectively) together with a decrease of the fibrosis-associated ARG1 marker (Fig.2D-E, -35%), and an increase of the anti-inflammatory marker CD206 (Fig.2E, +61%). The expression of CCR2 and CD301 was not affected (Fig.S2). Similarly, macrophages expressing pro-inflammatory markers were reduced in the diaphragm (Fig.2F, -23 and -31% for TNF $\alpha$  and iNOS, respectively), although the expression of ARG1 and CD206 was not affected in this muscle (Fig.2F). These results show that NaHS treatment specifically reduces the number of pro-inflammatory macrophages in mdx mice muscles.

### **Pharmacological dampening of macrophage pro-inflammatory phenotype by NaHS reduces myofiber branching in mdx mice**

To study the impact of pro-inflammatory macrophage reduction in dystrophic muscles, several myogenic parameters were analyzed after NaHS treatment. Immunostainings performed on TA transversal sections from treated mdx muscles did not show a modification of the number of satellite cells per fiber as determined by Pax7 immunostaining (Fig.S3A), or of the proportion of newly formed myofibers that expressed eMHC+ (Fig.S3B). However, NaHS treatment led to a decreased number of nuclei per myofiber in the TA (Fig.3A-B and Fig.S3C, -20 to -33% depending on the section level), as well as in the diaphragm (Fig.3C, -32%), suggesting a reduction in cell fusion. Importantly, this was confirmed by longitudinal analyses on mono-myofibers isolated from TA that showed a decrease in the number of nuclei/ $\mu\text{m}$  along the length of myofibers from NaHS-treated animals (Fig.3D-E, -8%). Muscle regeneration after an injury is associated with myofiber branching (Pichavant and Pavlath, 2014), which is characterized by myofibers containing two or more cytoplasmically continuous strands. Mdx mice harbor an increased proportion of branched myofibers as compared with wild-type (Bockhold et al., 1998), likely due to the permanent cycles of injury/regeneration, which is correlated with a decrease in muscle force production (Chan et al., 2007). Interestingly, isolated myofibers from NaHS-treated mdx mice were characterized by a decrease in myofiber branching (Fig.3F-G, 16% decrease). Altogether, these results show that dampening the pro-inflammatory status of macrophages is associated with a reduction of myofiber branching and of the number of myonuclei per myofiber, indicative of a reduction of muscle damage.

### **NaHS treatment improves dystrophic muscle**

Next, we evaluated the consequence of dampening the macrophage pro-inflammatory status by NaHS treatment on dystrophic muscle features. Hematoxylin-eosin (HE) staining of muscle transversal sections showed a strong decrease in the damaged areas in NaHS-treated mice in the TA (Fig.4A-B and Fig.S4A, -50 to -55% depending on the section level) and the diaphragm (Fig.4C, -58%). This was associated with a decrease in muscle fibrosis, as shown by the reduction in the areas expressing Collagen1 (Coll1) in the TA (Fig.4D-E and Fig.S4B, -9 to -10% depending on the section level), but not in the diaphragm (Fig.4F). Finally, the mean

cross-sectional area (CSA) of myofibers, which is correlated with muscle force production, was increased in the TA (Fig.4G-H and Fig.S4C, +18 to +27% depending on the section level) and the diaphragm (Fig.4I, +25%). Precisely, a decreased proportion of the smallest fibers (Fig.4G-H and Fig.S4C, -28% of fibers with CSA  $<500 \mu\text{m}^2$  on both TA section levels; Fig.4I, -23% of fibers with CSA  $<250 \mu\text{m}^2$  in the diaphragm) and a concomitant increased proportion of the bigger fibers (Fig.4G-H and Fig.S4C, +40 to +47% of fibers with CSA  $>5000 \mu\text{m}^2$  depending on the TA section level; Fig.4I, +155% of fibers with CSA between 2000 and  $2250 \mu\text{m}^2$  in the diaphragm) were observed in NaHS-treated mdx mice.

Taken together, these results show that the reduction of pro-inflammatory macrophages by NaHS treatment is associated with an amelioration of the dystrophic muscle phenotype.

### **AMPK $\alpha$ 1 is required for NaHS-induced dampening of pro-inflammatory macrophages**

The AMPK metabolic sensor plays a critical role in macrophage phenotypic shift during skeletal muscle regeneration (Mounier et al., 2013). As AMPK was previously shown to be activated by NaHS in a microglia cell line (Zhou et al., 2014), we asked whether NaHS-mediated pro-inflammatory macrophage dampening was mediated through AMPK activation. Treatment of wild-type BMDMs by NaHS increased the phosphorylation at Thr172 of the AMPK catalytic  $\alpha$  subunit after 1 and 2 h (Fig.5A-B, +61 and +89% as compared with untreated control, respectively), as did the AMPK allosteric activator 991 (Fig.5A-B, +80 and +110% as compared with untreated control, respectively), indicating AMPK activation. Next, we investigated the functional role of AMPK activation in NaHS-mediated macrophage skewing towards an anti-inflammatory phenotype. To this aim, we used AMPK $\alpha$ 1<sup>-/-</sup> BMDMs, which harbor a knockout in the gene coding for the AMPK  $\alpha$ 1 subunit, the only catalytic subunit expressed in macrophages (Sag et al., 2008) (Fig.5C). As expected, NaHS-induced AMPK activation was associated with a decreased expression of the pro-inflammatory markers TNF $\alpha$  and CCL3 (Fig.5D, -14 and -11%, respectively), and an increased expression of the anti-inflammatory markers CD206 and CD163 (Fig.5E, +19 and +11%, respectively). These NaHS-

mediated effects on macrophage inflammatory status were completely abrogated in AMPK $\alpha$ 1<sup>-/-</sup> BMDMs (Fig.5D). Finally, we used an *in vitro* model of adult myogenesis where conditioned medium generated from BMDMs was transferred onto MuSCs to stimulate their fusion into multinucleated myotubes (Fig.5F). Conditioned medium from NaHS-treated wild-type BMDMs increased MuSC fusion into myotubes (Fig.5G-H, +22%), whereas this was not observed with conditioned medium derived from NaHS-treated AMPK $\alpha$ 1<sup>-/-</sup> BMDMs (Fig.5G-H).

These results identify AMPK activation through the phosphorylation of its  $\alpha$ 1 catalytic subunit as a critical downstream target of NaHS in macrophages.

## **Discussion**

In the present study, we analyzed the interaction between myofibers and macrophages in the context of DMD. We showed that the dystrophic myofibers themselves skew resting macrophages towards a pro-inflammatory phenotype. As alterations in the secretome of myotubes generated by myoblasts isolated from mdx mice (Duguez et al., 2013) or DMD patients (Lecompte et al., 2017) have already been described, this suggests that in the context of degenerative myopathies, not only the degenerating/regenerating events lead to chronic inflammation, but the myofibers themselves contribute to the maintenance of the pro-inflammatory environment that alters macrophage properties and favors the generation of a pro-fibrotic population. Although the molecular effectors secreted by mdx myofibers contributing to the sustained inflammation remain to be precisely characterized, Duguez et al. showed an increased secretion of various proteins, including secreted protein acidic and rich in cysteine (SPARC), by myotubes derived from mdx-isolated myoblasts (Duguez et al., 2013). As *in vitro* treatment of peritoneal macrophages with recombinant SPARC was shown to stimulate the expression of pro-inflammatory genes such as *Tnfa* (Toba et al., 2015), its increased secretion by mdx myofibers could contribute to the skewing of resting macrophages towards a pro-inflammatory phenotype and, therefore, to fibrosis establishment in DMD muscle. Indeed, we previously showed that pro-inflammatory macrophages promote fibrosis in DMD muscle (Juban et al., 2018). Moreover, modulating the inflammatory status of this

population towards an anti-inflammatory phenotype improves DMD muscle function (Juban et al., 2018). Therefore, identification of specific anti-inflammatory strategies appears as a relevant therapeutic approach to alleviate muscle damage.

H<sub>2</sub>S is a gasotransmitter that exhibit anti-inflammatory properties, in part through the regulation of macrophage inflammatory status (Sun et al., 2020; Wallace et al., 2012). H<sub>2</sub>S donors have been widely used *in vivo* using animal models to treat various pathological conditions (Fagone et al., 2018). This includes reduction by the H<sub>2</sub>S donor NaHS of skeletal muscle atrophy in a mouse model of diabetes (Lu et al., 2020), or the decrease of muscle fibrosis after contusion-induced injury (Zhao et al., 2020). Interestingly, various therapeutics like Zofenopril have been shown to exert their effect through the indirect release of H<sub>2</sub>S (Fagone et al., 2018; Wallace et al., 2018). Recently, clinical studies have shown the safety and efficiency of H<sub>2</sub>S-releasing molecules in human. Patients with congestive heart failure exhibit a deficit of H<sub>2</sub>S in the blood. Treatment with the H<sub>2</sub>S donor SG1002 attenuated the level of brain natriuretic peptide, a stress marker of cardiac function, thus reducing the severity of and potentially preventing heart failure (Polhemus et al., 2015). Similarly, ATB-346, an H<sub>2</sub>S-releasing derivative of the nonsteroidal anti-inflammatory drug Naproxen, reduced the symptoms severity in osteoarthritis patients with reduced adverse effects as compared to Naproxen alone (Wallace et al., 2018; Wallace et al., 2020).

At the molecular level, the H<sub>2</sub>S donor NaHS was shown to favor microglia inflammatory shift towards an anti-inflammatory phenotype (Du et al., 2014; Zhou et al., 2014) through the activation of AMPK (Zhou et al., 2014). Interestingly, our previous work identified AMPK as a crucial activator of macrophage inflammatory shift during normal skeletal muscle regeneration (Mounier et al., 2013). In the present study, we identified AMPK as a critical mediator of NaHS-induced macrophage skewing that allow the acquisition of a phenotype associated with muscle repair. Although the molecular cascade leading to AMPK activation by NaHS in macrophages remains to be established, the resolvin Annexin A1 (ANXA1) may be involved in this process. Indeed, NaHS-induced down-regulation of pro-inflammatory markers expression in BMDMs following LPS stimulation requires the resolvin Annexin A1 (Brancaleone et al., 2014), and we

recently showed ANXA1 to trigger AMPK activation in macrophages through the binding of its G protein-coupled formyl peptide receptor (FPR) 2 (McArthur et al., 2020).

Thus, in an attempt to counteract the exacerbated macrophage pro-inflammatory phenotype induced by dystrophic myofibers, we treated mdx mice with NaHS. We showed that NaHS-treated mdx mice exhibited a decrease in the total number of macrophages in the TA and the diaphragm. More specifically, in the TA, we observed a reduction in the number of macrophages expressing pro-inflammatory markers as well as the ARG1 fibrotic marker, together with an increase in the anti-inflammatory CD206 marker, suggesting a skewing towards an anti-inflammatory phenotype and a reduction of the pro-fibrotic macrophage population (Juban et al., 2018). This was associated with a global muscle phenotype amelioration characterized by a reduced myofiber necrosis and reduced fibrosis, together with an increased myofiber size. In the diaphragm, NaHS treatment also induced a reduction of macrophages expressing pro-inflammatory markers but no effect was observed on ARG1 and CD206 markers. This was associated with a decreased myofiber necrosis and an increased myofiber size, but no fibrosis reduction. These discrepancies observed between the TA and the diaphragm may be explained by the more severe phenotype exhibited by the diaphragm, notably the higher level of fibrosis that may require extended treatment duration to be reduced. Globally, these results are in accordance with the beneficial effect observed on dystrophic muscle function by preventing the entry of circulating monocytes at early time points (Liang et al., 2018; Mojumdar et al., 2014; Wehling et al., 2001), or by skewing macrophage towards an anti-inflammatory phenotype (Juban et al., 2018). These results confirm that the modulation of macrophage inflammatory status is a relevant therapeutic approach to relieve inflammation and muscle damage in degenerative myopathies.

The amelioration of the muscle phenotype by NaHS treatment was characterized by a decrease in the number of nuclei per myofiber together with a reduction of myofiber branching. Branched myofibers are barely observed in normal skeletal muscle but they appear after regeneration following acute injury (Pichavant and Pavlath, 2014). They are observed in DMD patients (Bell and Conen, 1968) and in DMD fibers generated *in vitro* (Tanoury et al., 2020),

as well as in the mdx mouse model (Head et al., 1992; Lefaucheur et al., 1995). Branched myofibers are characterized by an impairment of calcium signaling and Excitation-Contraction coupling, causing myofiber function defects and higher fragility (Head, 2010; Lovering et al., 2009). While the mechanisms resulting in myofiber branching are still unclear (defect in final fusion between forming myofibers, or normal process that is exacerbated in dystrophic muscle due to continuous regeneration processes), a recent study showed in the mdx EDL muscle that the increased number of myonuclei per myofiber is concomitant to myofiber branching (Massopust et al., 2020). Accordingly, the concomitant reduction of the number of nuclei per myofiber and of branching observed in NaSH-treated mice suggests an improvement in muscle homeostasis.

To conclude, the present study identified a novel property of dystrophic myofibers in the DMD mouse model mdx, associated with a regulatory loop between myofibers and macrophages. Dystrophic myofibers skew macrophages towards a pro-inflammatory phenotype that in turn contributes to myofiber damage, consequently increasing myofiber branching and fragility, thus favoring muscle damage and fibrosis. Finally, this work identified H<sub>2</sub>S-releasing molecules as potential therapeutic strategies to dampen inflammation in DMD and improve dystrophic muscle phenotype through AMPK activation.

## **Materials and methods**

**Mice experiments.** DMD<sup>mdx4Cv</sup> (Chapman et al., 1989) mice on C57BL/6J background and 129;B6-Prkaa1<sup>tm</sup> (AMPK $\alpha$ 1<sup>-/-</sup>) were bred and used according to French legislations. The protocols were approved by the Ethical committee from Université Claude Bernard Lyon 1 (CEEA55). Experiments were conducted on males at 10-12 weeks of age. NaHS (1 mg/kg, Sigma-Aldrich) or PBS was injected daily intraperitoneally in mdx mice for 3 weeks and muscles were harvested the day after the last injection.

**Histology and immunofluorescence analyses in mouse.** Fascia of TA muscles was removed, then TA and diaphragm were frozen in nitrogen-chilled isopentane and kept at -80°C until use. 8  $\mu$ m-thick cryosections were prepared for HE staining and immunolabelings. For

immunolabelings, cryosections were permeabilized 10 min in 0.5 % Triton X-100 and saturated in 2% bovine serum albumin (BSA) for 1 h at room temperature. For identification of regenerating myofibers, saturated cryosections were co-labeled with primary antibodies directed against embryonic myosin (eMHC, sc-53091, Santa Cruz, 1/100) and Laminin (L9393, Sigma Aldrich, 1/200). For macrophage double immunolabelings, cryosections were labeled with antibodies (from Abcam unless indicated) against F4/80 (ab6640 or ab74383, 1/400) overnight at 4°C and labeling using the second antibody was performed for 2 h at 37°C. Antibodies were directed against Arginase 1 (sc-18355, Santa Cruz, 1/100), CCR2 (ab32144, 1/200), CD206 (sc-58987, Santa Cruz, 1/100), CD301 (ab59167, 1/200), Collagen I (ab292, ab34710 or Biotech 131001, 1/200), Cox2 (ab2372, 1/50), iNOS (ab15323, 1/25), Laminin (L9393, Sigma Aldrich, or ab78287, 1/200) and TNF $\alpha$  (ab34839, 1/50). Secondary antibodies were coupled to FITC, Cy3 or Cy5 (Jackson Immunoresearch Inc, 1/200). Muscle stem cells were labeled as previously described (Th  ret et al., 2017) using an antibody directed against Pax7 (AB\_528428, DSHB, 1/10). HE-stained muscle sections were recorded with a Nikon E800 microscope at 20X magnification connected to a QIMAGING camera. Damaged areas were measured as previously described (Juban et al., 2018). Fluorescent immunolabelings were recorded with a DMI 6000 Leica microscope connected to a Coolsnap camera at 20X magnification. For each condition of each experiment, at least 8-10 fields chosen randomly were counted. The number of labeled macrophages was calculated using the Image J software and was expressed as a percentage of total macrophages. Areas of Collagen1 were calculated with ImageJ software as previously described (Juban et al., 2018). Cross Section Area (CSA) was determined on whole muscle sections labeled by laminin antibody using Open-CSAM program as previously described (Desgeorges et al., 2019). For quantification in the TA of the number of nuclei per myofiber, damaged areas, fibrotic areas and CSA, 2 different cross sections were analyzed in TA muscles. The first and second cross sections were harvested 5 and 10 mm from the tendon base, respectively.

**Murine BMDM isolation and culture.** Macrophages were derived from murine bone marrow precursors as previously described (Mounier et al., 2013). Briefly, total bone marrow

was obtained by flushing femur and tibiae from wild-type C57BL/6J mice with Dubecco's Modified Eagle's Medium (DMEM). Cells were cultured in DMEM containing 20% heat inactivated Fetal Bovine Serum (FBS), 30% of L929 cell line-derived conditioned medium (enriched in CSF-1), 2.5 µg/mL of fungizone and 100 U/mL of penicillin/streptomycin for 6-7 days. To generate conditioned medium, 110,000 cells/cm<sup>2</sup> were treated with 500 µM NaHS for 2 days. Cells were then washed twice with PBS and incubated for 24 h in DMEM F-12 medium (Gibco) without serum. Medium was collected, centrifuged for 10 min at 500 g and supplemented with 2% Horse serum (HS, Gibco) before transfer onto MuSC culture (see below).

**Murine BMDM immunophenotypic characterization.** 54,000 cells/cm<sup>2</sup> were seeded on glass coverslips and treated by 500 µM of NaHS for 2 days. Cells were fixed for 10 min in 4% formaldehyde, permeabilized 10 min in 0.5 % Triton X-100 and saturated in 2% BSA for 1 h at room temperature. They were then labeled as described above with anti-TNFα (ab34839, 1/50), anti-CCL3 (sc-1383, Santa Cruz, 1/50), anti-CD206 (ab64693, 1/50) or anti-CD163 (bs-2527R, Bioss, 1/100) primary antibodies revealed by secondary antibodies coupled to FITC or Cy3 (Jackson ImmunoResearch Inc, 1/200). After nuclei staining with Hoechst, cells were mounted in Fluoromount (Interchim) and 10 to 12 random fields were imaged on a Nikon E800 microscope at 10X magnification connected to a QIMAGING camera.

**Cocultures of macrophages with isolated single myofibers.** Single myofibers of *extensor digitorum longus* (EDL) muscle were isolated from wild-type and mdx mice as previously described (Le Grand et al., 2012) and were cocultured as 15 myofibers/well in 96 wells containing 14000 cells/cm<sup>2</sup> of wild-type bone-marrow derived macrophages (prepared as described above) for 3 days. Macrophages were immunolabelled as described above for the immunofluorescence on muscle sections. For each condition of each experiment, about 10-12 fields chosen randomly were recorded with a DMI 6000 Leica microscope connected to a Coolsnap camera (Photometrics) at 20X magnification.

**Isolation of single myofibers from TA muscle.** Fascia of TA muscles was removed and muscles were fixed for 45 min in 4% formaldehyde. After 2 quick washes and a 30 min wash

in PBS, muscles were transferred into PBS containing 0.5% Triton X-100. 30 to 40 single myofibers were gently isolated by manual dissociation using tweezers, incubated with 1 $\mu$ g/mL of Hoechst to label their nuclei, and mounted on slides. Slides were observed on an Axio Observer.Z1 (Zeiss) connected to a CoolSNAP HQ2 CCD Camera (Photometrics) and the branched myofibers were numerated. For the quantification of the number of nuclei, between 30 and 40 images corresponding to 7,000-9,000 nuclei from 6 to 10 randomly chosen single myofibers were acquired and the number of nuclei was normalized by the myofiber length.

**Isolation and culture of MuSCs.** Muscle hindlimbs from adult males were dissociated and digested first for 45 min at 37°C under agitation in Ham's F-10 medium (Gibco) containing 10% HS (Gibco) and 300 U/mL collagenase II (Gibco), followed by a second digestion for 30 min at 37°C under agitation in Ham's F-10 medium (Gibco) containing 10% HS (Gibco), 150 U/mL collagenase II (Gibco) and 1,7 U/mL dispase (Gibco). MuSCs were isolated with Satellite Cell Isolation Kit (Miltenyi Biotec) using LS Columns (Miltenyi Biotec) on a MidiMACS separator (Miltenyi Biotec), and seeded on gelatin-coated flasks at 2,000 cells/cm<sup>2</sup> in DMEM F-12 (Gibco) supplemented with 20% FBS, 2% Ultrosor G (Pall Gelman Sciences) and 100 U/mL of penicillin/streptomycin.

**MuSC fusion assay.** MuSCs were seeded on Growth Factor Reduced Matrigel (Corning) at 10,000 cells/cm<sup>2</sup> in DMEM F-12 (Gibco) supplemented with 20% FBS, 2% Ultrosor G (Pall Gelman Sciences) and 100 U/mL of penicillin/streptomycin overnight and culture medium was replaced by macrophage-derived conditioned medium (see above). After 48 h, cells were fixed for 10 min in 4% formaldehyde, permeabilized 10 min in 0.5 % Triton X-100 and saturated in 2% BSA for 1 h at room temperature. They were then labeled and mounted as described above with an anti-desmin antibody (ab32362, 1/200). Ten to 12 random fields were imaged on a Nikon E800 microscope at 10X magnification connected to a QIMAGING camera.

**Western blot.** Two million macrophages were seeded in 6-well plates. One h before treatment, culture medium was replaced by DMEM without red phenol (Gibco) supplemented with 10% charcoal stripped FBS (Gibco) and cells were treated with 10  $\mu$ M 991 (SpiroChem) or 500  $\mu$ M NaHS (Sigma Aldrich) for 1 or 2 h. Proteins were isolated in lysis buffer containing

50 mM Tris-HCL (pH 7.5), 1 mM EDTA, 1 mM EGTA, 0.27 M sucrose, 1% triton, 20 mM glycerol-2- phosphate disodium, 50 mM NaF, 0.5 mM PMSF, 1 mM benzamidine, 1 mM Na<sub>3</sub>VO<sub>4</sub> and 1% cocktail phosphatase inhibitor 3 (Sigma-Aldrich, P0044) for 30 min on ice and centrifuged for 10 min at 16,100 g to remove debris. Twenty five µg of proteins were subjected to SDS-PAGE and transferred onto a nitrocellulose membrane which was probed with antibodies against p-AMPK $\alpha$  (#2531, Cell Signaling, 1/1000), AMPK $\alpha$  (#2532, Cell Signaling, 1/1000), or  $\beta$ -actin (A5316, Sigma-Aldrich, 1/2000). Blots were revealed on a Chemidoc imager (Bio-Rad) using SuperSignal West Femto Maximum Sensitivity Substrate (Thermo Scientific) and signal intensity was quantified using Image Lab Software (Bio-Rad).

**Statistical Analyses.** All experiments were performed using at least three different cultures or animals in independent experiments. Statistical tests were performed using GraphPad Prism. Depending on the experimental setup, Student's t test, one-way or two-way ANOVA with multiple comparisons were used for statistical analyses.

### **Acknowledgements**

This work was funded by the Framework Programme FP7 Endostem (under grant agreement 241440), Association Française contre les myopathies (MyoNeurAlp Alliance) and Fondation pour la Recherche Médicale (Equipe FRM DEQ20140329495).

### **Conflict of interest**

The authors declare that they have no conflict of interest

### **Author contribution**

Conceptualization: GJ, BC, RM; Methodology: MS, SBL, GJ, HML, EM, BC; Analysis: SBL, GJ, MS, BC; Writing original draft: GJ, MS; Writing review & editing: GJ, MS, BC, RM; Supervision: GJ, BC; Funding Acquisition: BC, GJ.

## References

- Acharyya, S., Villalta, S. A., Bakkar, N., Bupha-Intr, T., Janssen, P. M. L., Carathers, M., Li, Z.-W., Beg, A. A., Ghosh, S., Sahenk, Z., et al. (2007).** Interplay of IKK/NF-kappaB signaling in macrophages and myofibers promotes muscle degeneration in Duchenne muscular dystrophy. *J. Clin. Invest.* **117**, 889–901.
- Arnold, L., Henry, A., Poron, F., Baba-Amer, Y., van Rooijen, N., Plonquet, A., Gherardi, R. K. and Chazaud, B. (2007).** Inflammatory monocytes recruited after skeletal muscle injury switch into antiinflammatory macrophages to support myogenesis. *J. Exp. Med.* **204**, 1057–1069.
- Bell, C. D. and Conen, P. E. (1968).** Histopathological changes in Duchenne muscular dystrophy. *J. Neurol. Sci.* **7**, 529–544.
- Bentzinger, C. F., Wang, Y. X., Dumont, N. A. and Rudnicki, M. A. (2013).** Cellular dynamics in the muscle satellite cell niche. *EMBO Rep.* **14**, 1062–1072.
- Bockhold, K. J., Rosenblatt, J. D. and Partridge, T. A. (1998).** Aging normal and dystrophic mouse muscle: analysis of myogenicity in cultures of living single fibers. *Muscle Nerve* **21**, 173–183.
- Brancaleone, V., Mitidieri, E., Flower, R. J., Cirino, G. and Perretti, M. (2014).** Annexin A1 mediates hydrogen sulfide properties in the control of inflammation. *J. Pharmacol. Exp. Ther.* **351**, 96–104.
- Calvert, J. W., Coetzee, W. A. and Lefer, D. J. (2010).** Novel insights into hydrogen sulfide--mediated cytoprotection. *Antioxid Redox Signal* **12**, 1203–1217.
- Chan, S., Head, S. I. and Morley, J. W. (2007).** Branched fibers in dystrophic mdx muscle are associated with a loss of force following lengthening contractions. *Am. J. Physiol. Cell*

*Physiol.* **293**, C985–92.

**Chapman, V. M., Miller, D. R., Armstrong, D. and Caskey, C. T.** (1989). Recovery of induced mutations for X chromosome-linked muscular dystrophy in mice. *Proc. Natl. Acad. Sci. U.S.A.* **86**, 1292–1296.

**Dadgar, S., Wang, Z., Johnston, H., Kesari, A., Nagaraju, K., Chen, Y.-W., Hill, D. A., Partridge, T. A., Giri, M., Freishtat, R. J., et al.** (2014). Asynchronous remodeling is a driver of failed regeneration in Duchenne muscular dystrophy. *J. Cell Biol.* **207**, 139–158.

**Desgeorges, T., Liot, S., Lyon, S., Bouvière, J., Kemmel, A., Trignol, A., Rousseau, D., Chapuis, B., Gondin, J., Mounier, R., et al.** (2019). Open-CSAM, a new tool for semi-automated analysis of myofiber cross-sectional area in regenerating adult skeletal muscle. *Skelet. Muscle* **9**, 2.

**Du, C., Jin, M., Hong, Y., Li, Q., Wang, X.-H., Xu, J.-M., Wang, F., Zhang, Y., Jia, J., Liu, C.-F., et al.** (2014). Downregulation of cystathionine  $\beta$ -synthase/hydrogen sulfide contributes to rotenone-induced microglia polarization toward M1 type. *Biochem. Biophys. Res. Commun.* **451**, 239–245.

**Duguez, S., Duddy, W., Johnston, H., Lainé, J., Le Bihan, M. C., Brown, K. J., Bigot, A., Hathout, Y., Butler-Browne, G. and Partridge, T.** (2013). Dystrophin deficiency leads to disturbance of LAMP1-vesicle-associated protein secretion. *Cell. Mol. Life Sci.* **70**, 2159–2174.

**Fagone, P., Mazzon, E., Bramanti, P., Bendtzen, K. and Nicoletti, F.** (2018). Gasotransmitters and the immune system: Mode of action and novel therapeutic targets. *Eur. J. Pharmacol.* **834**, 92–102.

**Head, S. I.** (2010). Branched fibres in old dystrophic mdx muscle are associated with mechanical weakening of the sarcolemma, abnormal Ca<sup>2+</sup> transients and a breakdown of

Ca<sup>2+</sup> homeostasis during fatigue. *Exp. Physiol.* **95**, 641–656.

**Head, S. I., Williams, D. A. and Stephenson, D. G.** (1992). Abnormalities in structure and function of limb skeletal muscle fibres of dystrophic mdx mice. *Proc. Biol. Sci.* **248**, 163–169.

**Juban, G., Saclier, M., Yacoub-Youssef, H., Kernou, A., Arnold, L., Boisson, C., Ben Larbi, S., Magnan, M., Cuvellier, S., Théret, M., et al.** (2018). AMPK activation regulates LTBP4-dependent TGF-beta;1 secretion by pro-inflammatory macrophages and controls fibrosis in duchenne muscular dystrophy. *Cell Rep.* **25**, 2163–2176.

**Lapidos, K. A., Kakkar, R. and McNally, E. M.** (2004). The dystrophin glycoprotein Complex: signaling strength and integrity for the sarcolemma. *Circ. Res.* **94**, 1023–1031.

**Latroche, C., Weiss Gayet, M., Muller, L., Gitiaux, C., Leblanc, P., Liot, S., Ben Larbi, S., Abou-Khalil, R., Verger, N., Bardot, P., et al.** (2017). Coupling between myogenesis and mngiogenesis during skeletal muscle regeneration is stimulated by restorative macrophages. *Stem Cell Reports* **9**, 1–16.

**Le Grand, F., Grifone, R., Mourikis, P., Houbron, C., Gigaud, C., Pujol, J., Maillet, M., Pagès, G., Rudnicki, M., Tajbakhsh, S., et al.** (2012). Six1 regulates stem cell repair potential and self-renewal during skeletal muscle regeneration. *J. Cell Biol.* **198**, 815–832.

**Lecompte, S., Abou-Samra, M., Boursereau, R., Noel, L. and Brichard, S. M.** (2017). Skeletal muscle secretome in Duchenne muscular dystrophy: a pivotal anti-inflammatory role of adiponectin. *Cell. Mol. Life Sci.* **74**, 2487–2501.

**Lefaucheur, J. P., Pastoret, C. and Sebille, A.** (1995). Phenotype of dystrophinopathy in old mdx mice. *Anat. Rec.* **242**, 70–76.

**Lemos, D. R., Babaeijandaghi, F., Low, M., Chang, C.-K., Lee, S. T., Fiore, D., Zhang, R.-H., Natarajan, A., Nedospasov, S. A. and Rossi, F. M. V.** (2015). Nilotinib reduces

muscle fibrosis in chronic muscle injury by promoting TNF-mediated apoptosis of fibro/adipogenic progenitors. *Nat. Med.* **21**, 786–794.

**Liang, F., Giordano, C., Shang, D., Li, Q. and Petrof, B. J.** (2018). The dual CCR2/CCR5 chemokine receptor antagonist Cenicriviroc reduces macrophage infiltration and disease severity in Duchenne muscular dystrophy (Dmdmdx-4Cv) mice. *PLoS One* **13**, e0194421.

**Lovering, R. M., Michaelson, L. and Ward, C. W.** (2009). Malformed mdx myofibers have normal cytoskeletal architecture yet altered EC coupling and stress-induced Ca<sup>2+</sup> signaling. *Am. J. Physiol. Cell Physiol.* **297**, C571–C580.

**Lu, F., Lu, B., Zhang, L., Wen, J., Wang, M., Zhang, S., Li, Q., Shu, F., Sun, Y., Liu, N., et al.** (2020). Hydrogen sulphide ameliorating skeletal muscle atrophy in db/db mice via Muscle RING finger 1 S-sulfhydration. *J. Cell. Mol. Med.* **24**, 9362–9377.

**Massopust, R. T., Lee, Y., Pritchard, A. L., Nguyen, V.-K. M., McCreedy, D. A. and Thompson, W. J.** (2020). Lifetime analysis of mdx skeletal muscle reveals a progressive pathology that leads to myofiber loss. *Sci Rep* **10**, 1–16.

**McArthur, S., Juban, G., Gobbetti, T., Desgeorges, T., Théret, M., Gondin, J., Toller-Kawahisa, J. E., Reutelingsperger, C. P., Chazaud, B., Perretti, M., et al.** (2020). Annexin A1 drives macrophage skewing to accelerate muscle regeneration through AMPK activation. *J. Clin. Invest.* **130**, 1156–1167.

**McDonald, C. M., Henricson, E. K., Abresh, R. T., Duong, T., Joyce, N. C., Hu, F., Clemens, P. R., Hoffman, E. P., Cnaan, A., Gordish-Dressman, H., et al.** (2018). Long-term effects of glucocorticoids on function, quality of life, and survival in patients with Duchenne muscular dystrophy: a prospective cohort study. *Lancet* **391**, 451–461.

**Mojumdar, K., Liang, F., Giordano, C., Lemaire, C., Danialou, G., Okazaki, T., Bourdon, J., Rafei, M., Galipeau, J., Divangahi, M., et al.** (2014). Inflammatory monocytes promote

progression of Duchenne muscular dystrophy and can be therapeutically targeted via CCR2. *EMBO Mol. Med.* **6**, 1476–1492.

**Mounier, R., Théret, M., Arnold, L., Cuvelier, S., Bultot, L., Göransson, O., Sanz, N., Ferry, A., Sakamoto, K., Foretz, M., et al.** (2013). AMPK $\alpha$ 1 regulates macrophage skewing at the time of resolution of inflammation during skeletal muscle regeneration. *Cell Metab.* **18**, 251–264.

**Perdiguerro, E., Sousa-Victor, P., Ruiz-Bonilla, V., Jardí, M., Caelles, C., Serrano, A. L. and Muñoz-Cánoves, P.** (2011). p38/MKP-1-regulated AKT coordinates macrophage transitions and resolution of inflammation during tissue repair.. *J Cell Biol* **195**, 307–322.

**Pichavant, C. and Pavlath, G. K.** (2014). Incidence and severity of myofiber branching with regeneration and aging. *Skelet. Muscle* **4**, 9.

**Polhemus, D. J., Li, Z., Pattillo, C. B., Gojon, G., Sr, Gojon, G., Jr, Giordano, T. and Krum, H.** (2015). A Novel Hydrogen Sulfide Prodrug, SG1002, Promotes Hydrogen Sulfide and Nitric Oxide Bioavailability in Heart Failure Patients. *Cardiovasc. Ther.* **33**, 216–226.

**Ruffell, D., Mourkioti, F., Gambardella, A., Kirstetter, P., Lopez, R. G., Rosenthal, N. and Nerlov, C.** (2009). A CREB-C/EBPbeta cascade induces M2 macrophage-specific gene expression and promotes muscle injury repair. *Proc Natl Acad Sci U S A* **106**, 17475–17480.

**Saclier, M., Lapi, M., Bonfanti, C., Rossi, G., Antonini, S. and Messina, G.** (2020). The Transcription Factor Nfix Requires RhoA-ROCK1 Dependent Phagocytosis to Mediate Macrophage Skewing during Skeletal Muscle Regeneration. *Cells* **9**, 708–17.

**Saclier, M., Yacoub-Youssef, H., Mackey, A. L., Arnold, L., Ardjoune, H., Magnan, M., Sailhan, F., Chelly, J., Pavlath, G. K., Mounier, R., et al.** (2013). Differentially activated macrophages orchestrate myogenic precursor cell fate during human skeletal muscle

regeneration. *Stem Cells* **31**, 384–396.

**Schakman, O., Kalista, S., Barbé, C., Loumaye, A. and Thissen, J. P.** (2013).

Glucocorticoid-induced skeletal muscle atrophy. *Int. J. Biochem. Cell Biol.* **45**, 2163–2172.

**Sun, F., Luo, J. H., Yue, T. T., Wang, F. X., Yang, C. L., Zhang, S., Wang, X. Q. and Wang,**

**C. Y.** (2020). The role of hydrogen sulphide signalling in macrophage activation.

*Immunology* **109**, 1259–8.

**Tanoury, Z. A., Zimmermann, J. F., Rao, J., Sieiro, D., McNamara, H., Cherrier, T., Hick,**

**A., Bousson, F., Fugier, C., Marchiano, F., et al.** (2020). Prednisolone rescues

Duchenne Muscular Dystrophy phenotypes in human pluripotent stem cells-derived

skeletal muscle in vitro. *bioRxiv*, doi: 10.1101/2020.10.29.360826.

**Théret, M., Gsaier, L., Schaffer, B., Juban, G., Ben Larbi, S., Weiss Gayet, M., Bultot, L.,**

**Collodet, C., Foretz, M., Desplanches, D., et al.** (2017). AMPK $\alpha$ 1-LDH pathway

regulates muscle stem cell self-renewal by controlling metabolic homeostasis. *EMBO J.*

**36**, 1946–1962.

**Tonkin, J., Temmerman, L., Sampson, R. D., Gallego-Colon, E., Barberi, L., Bilbao, D.,**

**Schneider, M. D., Musarò, A. and Rosenthal, N.** (2016). Monocyte/Macrophage-derived

IGF-1 Orchestrates Murine Skeletal Muscle Regeneration and Modulates Autocrine

Polarization. *Mol Ther* **23**, 1189–1200.

**Vidal, B., Serrano, A. L., Tjwa, M., Suelves, M., Ardite, E., De Mori, R., Baeza-Raja, B.,**

**Martinez de Lagran, M., Lafuste, P., Ruiz-Bonilla, V., et al.** (2008). Fibrinogen drives

dystrophic muscle fibrosis via a TGF $\beta$  /alternative macrophage activation pathway.

*Genes Dev.* **22**, 1747–1752.

**Wallace, J. L., Ferraz, J. G. P. and Muscara, M. N.** (2012). Hydrogen Sulfide: An Endogenous

Mediator of Resolution of Inflammation and Injury. *Antioxid. Redox Signal.* **17**, 58–67.

- Wallace, J. L., Nagy, P., Feener, T. D., Allain, T., Ditrói, T., Vaughan, D. J., Muscara, M. N., de Nucci, G. and Buret, A. G.** (2020). A proof-of-concept, Phase 2 clinical trial of the gastrointestinal safety of a hydrogen sulfide-releasing anti-inflammatory drug. *Br. J. Pharmacol.* **177**, 769–777.
- Wallace, J. L., Vaughan, D., Dickey, M., MacNaughton, W. K. and de Nucci, G.** (2018). Hydrogen Sulfide-Releasing Therapeutics: Translation to the Clinic. *Antioxid. Redox Signal.* **28**, 1533–1540.
- Wang, R.** (2014). Gasotransmitters: growing pains and joys. *Trends Biochem. Sci.* **39**, 227–232.
- Wehling, M., Spencer, M. J. and Tidball, J. G.** (2001). A nitric oxide synthase transgene ameliorates muscular dystrophy in mdx mice. *J. Cell Biol.* **155**, 123–132.
- Wood, C. L., Straub, V., Guglieri, M., Bushby, K. and Cheetham, T.** (2015). Short stature and pubertal delay in Duchenne muscular dystrophy. *Arch. Dis. Child.* **101**, 101–106.
- Zhao, L., Liu, X., Zhang, J., Dong, G., Xiao, W. and Xu, X.** (2020). Hydrogen sulfide alleviates skeletal muscle fibrosis via attenuating inflammation and oxidative stress. *Front. Physiol.* **11**, 533690.
- Zhao, W., Wang, X., Ransohoff, R. M. and Zhou, L.** (2016). CCR2 deficiency does not provide sustained improvement of muscular dystrophy in mdx5c mice. *FASEB J.* **31**, 35–46.
- Zhou, X., Cao, Y., Ao, G., Hu, L., Liu, H., Wu, J., Wang, X., Jin, M., Zheng, S., Zhen, X., et al.** (2014). CaMKK $\beta$ -dependent activation of AMP-activated protein kinase is critical to suppressive effects of hydrogen sulfide on neuroinflammation. *Antioxid. Redox Signal.* **21**, 1741–1758.

## **Figure Legends**

**Figure 1. Dystrophic myofibers trigger pro-inflammatory macrophages. (A)** Diagram depicting the cocultures of BMDMs with isolated single myofibers. **(B-C)** BMDMs that were cultured alone (none) or with wild-type (WT) or mdx myofibers for 3 days were immunolabelled for pro- (TNF $\alpha$ , CCR2, COX2 and iNOS) or anti- (CD301, ARG1) inflammatory markers. **(B)** Representative images of TNF $\alpha$ , iNOS, COX2 and ARG1 immunolabelings. Scale bar, 50  $\mu$ m. Arrows indicate macrophages negative (white arrow) or positive (yellow arrow) for the specified marker. **(C)** Percentage of macrophages positive for the specified marker. Results are means  $\pm$  sem of 4-7 experiments. Statistical analysis was performed by one-way ANOVA with multiple comparisons, \* $p$ <0.05; \*\* $p$ <0.01; \*\*\* $p$ <0.001.

**Figure 2. NaHS treatment reduces pro-inflammatory macrophages in mdx muscle. (A)** Mdx mice were treated daily with PBS or NaHS for 3 weeks and TA and diaphragm muscles were harvested. **(B-C)** Muscle sections were immunostained for F4/80 and Laminin and the number of macrophages per myofiber was determined in the TA **(B)** and the diaphragm **(C)**. **(D-F)** Muscle sections were immunolabeled for F4/80 and pro- (TNF $\alpha$ , iNOS) or anti- (ARG1, CD206) inflammatory markers. **(D)** Representative images of F4/80 and TNF $\alpha$  (left panel), iNOS (middle panel) and ARG1 (right panel) immunolabelings in the TA. Arrows indicate macrophages negative (white arrow) or positive (yellow arrow) for the specified marker. Scale bar, 50  $\mu$ m. **(E-F)** Percentage of macrophages positive for the specified marker in the TA **(E)** and in the diaphragm **(F)**. Results are means  $\pm$  sem of 4-9 experiments. Statistical analyses were performed by Student's t test, \* $p$ <0.05; \*\* $p$ <0.01; \*\*\* $p$ <0.001.

**Figure 3. NaHS treatment reduces muscle damage in mdx mice.** Mdx mice were treated daily with PBS or NaHS for 3 weeks (as described in Fig.2A), TA and diaphragm muscles were harvested and immunostainings were performed. **(A-C)** Muscle sections were immunolabeled for Laminin and Hoechst to determine the number of nuclei per myofiber. **(A)** Representative

images of laminin and Hoechst immunolabeling in the TA. Scale bar, 50  $\mu\text{m}$ . **(B-C)** Number of nuclei per myofiber in the TA **(B)** and the diaphragm **(C)**. **(D-G)** Single myofibers were isolated from the TA and labeled with Hoechst to determine the number of nuclei and the proportion of branched myofibers. **(D)** Representative image of Hoechst labeling. Scale bar, 25  $\mu\text{m}$ . **(E)** Number of nuclei per  $\mu\text{m}$  of myofiber length. **(F)** Representative image of a branched myofiber. Scale bar, 100  $\mu\text{m}$ . **(G)** Percentage of branched myofibers. Results are means  $\pm$  sem of 5-7 experiments. Statistical analyses were performed by Student's t test, \* $p < 0.05$ .

**Figure 4. NaHS treatment ameliorates dystrophic muscle phenotype.** Mdx mice were treated daily with PBS or NaHS for 3 weeks (as described in Fig.2A) and TA and diaphragm muscles were harvested. **(A-C)** Muscle sections were stained with HE and the damaged area were determined. **(A)** Representative images of HE staining in the TA showing damaged areas circled in black. Scale bar, 50  $\mu\text{m}$ . **(B-C)** Percentage of damaged area per muscle section in the TA **(B)** or the diaphragm **(C)**. **(D-F)** Muscle sections were immunostained for Coll1. **(D)** Representative images of Coll1 immunostaining in the TA. Scale bar, 50  $\mu\text{m}$ . **(E-F)** Percentage of Coll1 area in the TA **(E)** or the diaphragm **(F)**. **(G-I)** Myofiber Cross-Section Area (CSA) was determined on whole muscle section after laminin immunolabeling. **(G)** Representative images of laminin immunolabeling in the TA. Scale bar, 50  $\mu\text{m}$ . **(H-I)** Mean CSA (top graph) and repartition of myofibers by size (bottom graph) in the TA **(H)** or the diaphragm **(I)**. Results are means  $\pm$  sem of 4-9 experiments. Statistical analyses were performed by Student's t test **(B, C, E, F, and H-I - bottom graphs)** or two-way ANOVA **(H and I - bottom graphs)** with multiple comparisons, \* $p < 0.05$ ; \*\* $p < 0.01$ .

**Figure 5. AMPK $\alpha$ 1 mediates NaHS-induced acquisition of the macrophage anti-inflammatory phenotype.** **(A-B)** BMDMs were treated with 991 or NaHS for 1-2 h and the phosphorylation of AMPK $\alpha$  on Thr172 was quantified by immunoblot. **(A)** Representative immunoblot. **(B)** Quantification of the ratio between the phosphorylated over the total

AMPK $\alpha$  protein. Each dot color represents an independent experiment. **(C-E)** WT and AMPK $\alpha$ 1<sup>-/-</sup> BMDMs were treated with NaHS for 48 h and immunolabelled for pro- (TNF $\alpha$  and CCL3) or anti- (CD206 and CD163) inflammatory markers. **(C)** Experimental set-up. **(D)** Percentage of macrophages positive for the pro-inflammatory markers TNF $\alpha$  and CCL3. **(E)** Percentage of macrophages positive for the anti-inflammatory markers CD206 and CD163. **(F-H)** Conditioned medium produced by WT and AMPK $\alpha$ 1<sup>-/-</sup> BMDMs treated with NaHS was transferred onto MuSCs and their fusion was assessed by immunofluorescence. **(F)** Experimental setup. **(G)** Representative images of desmin and Hoechst immunostaining of MuSC cultures. Arrows show nuclei from mononucleated (white arrow) or multinucleated cells (yellow arrow). Scale bar, 50  $\mu$ m. **(H)** Fusion index calculated as the percentage of nuclei in multinucleated cells over the total number of nuclei. Results are means  $\pm$  sem of 3-4 experiments. Statistical analyses were performed by one-way ANOVA **(B)** or two-way ANOVA **(D, E, H)** with multiple comparisons, \*p<0.05; \*\*p<0.01.

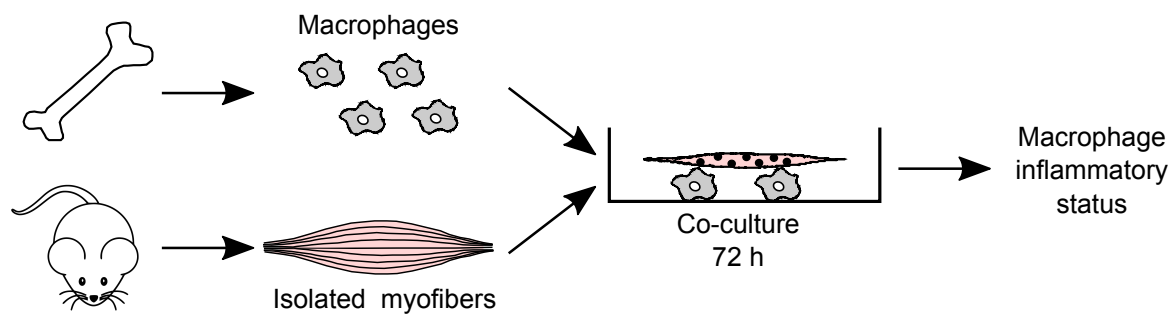
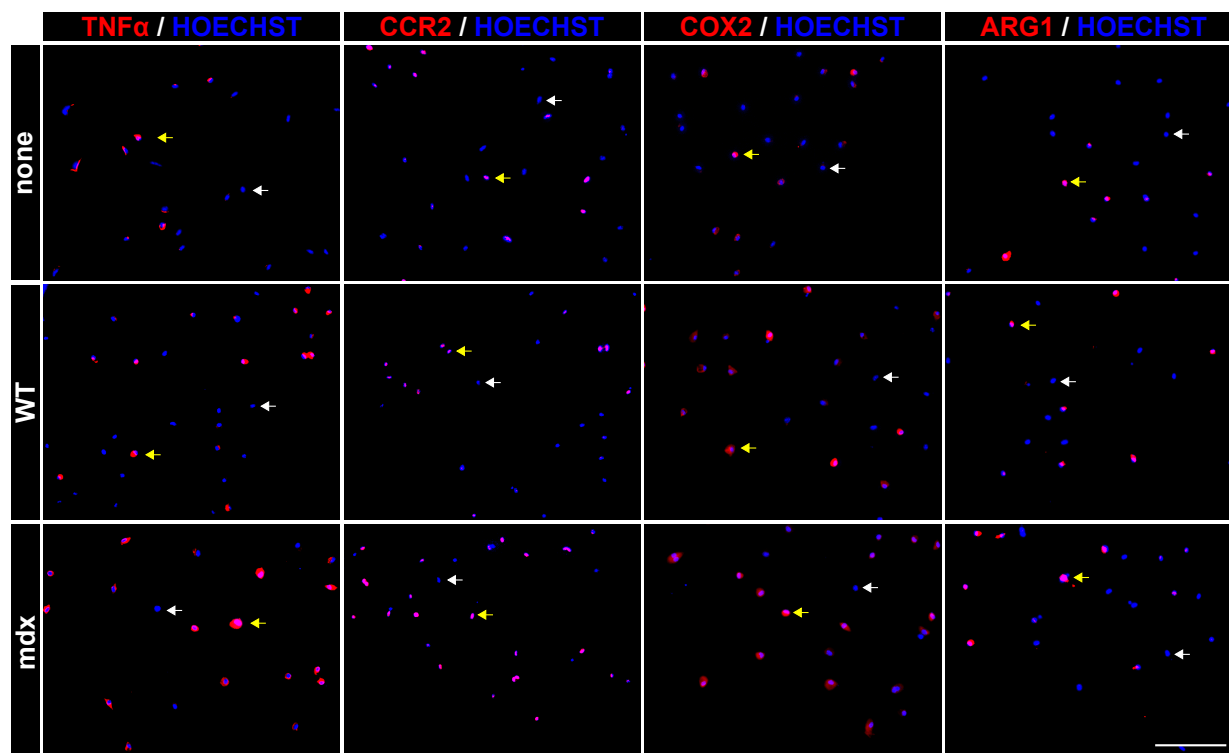
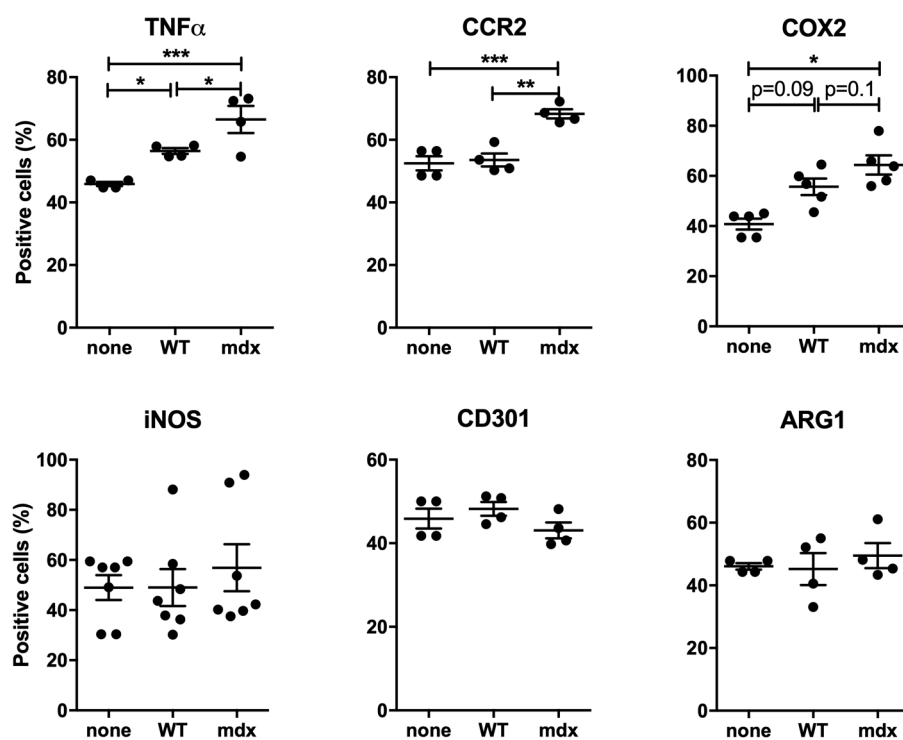
**A****B****C**

Figure 1

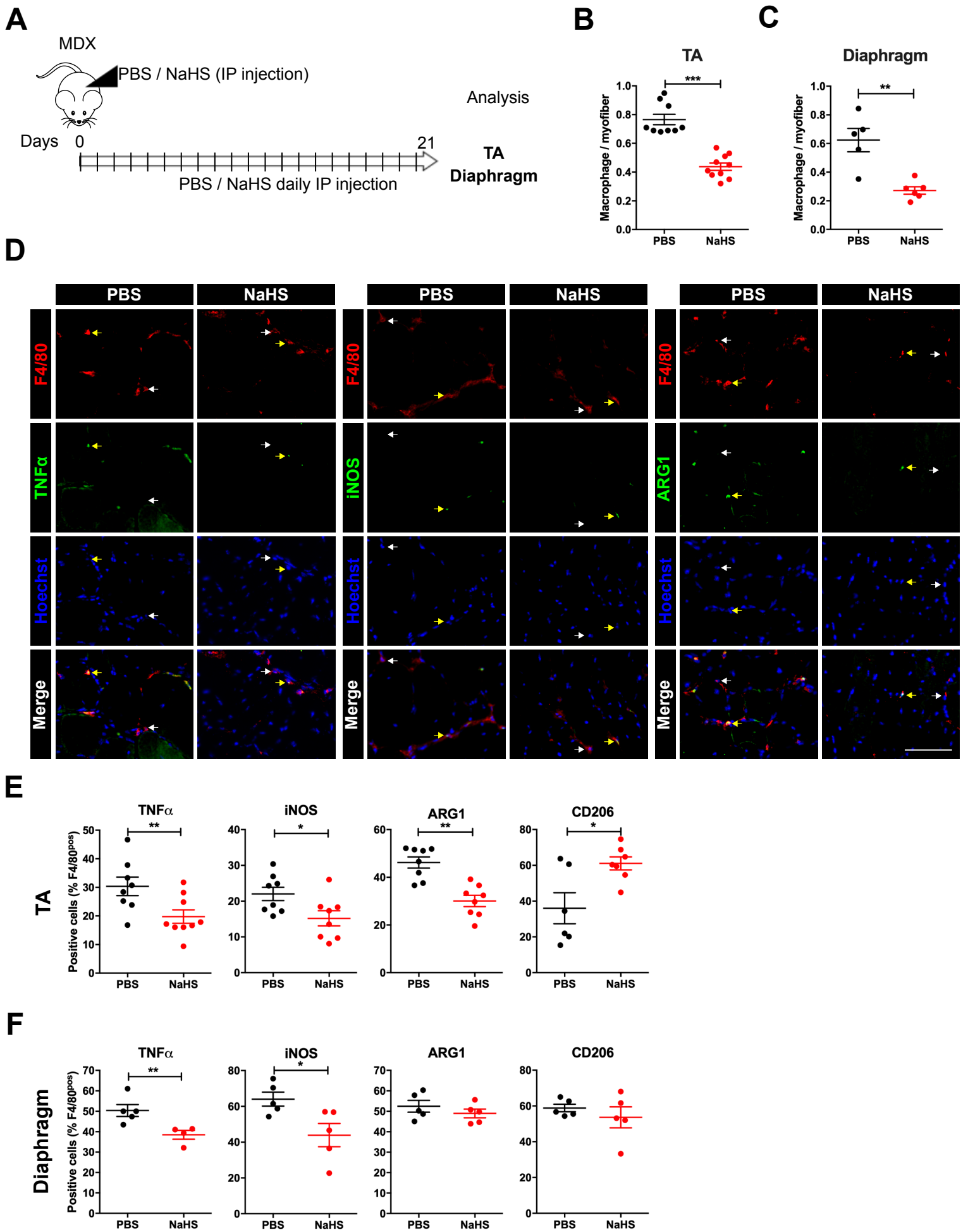
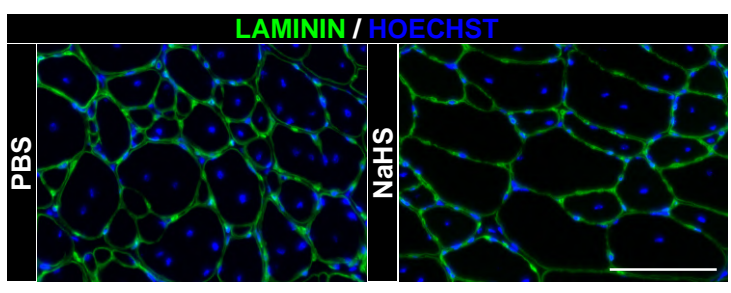
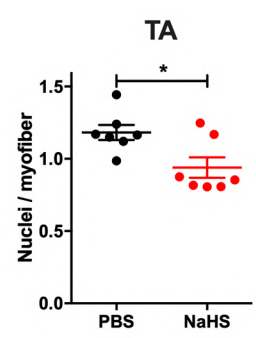
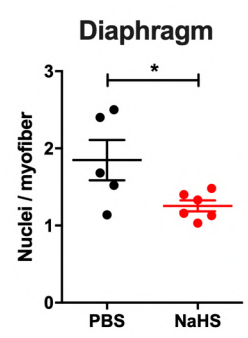
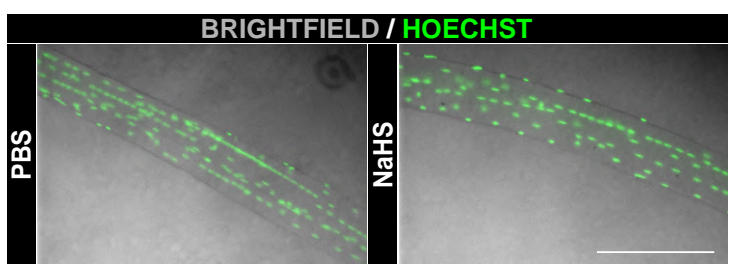
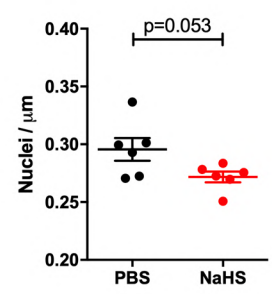
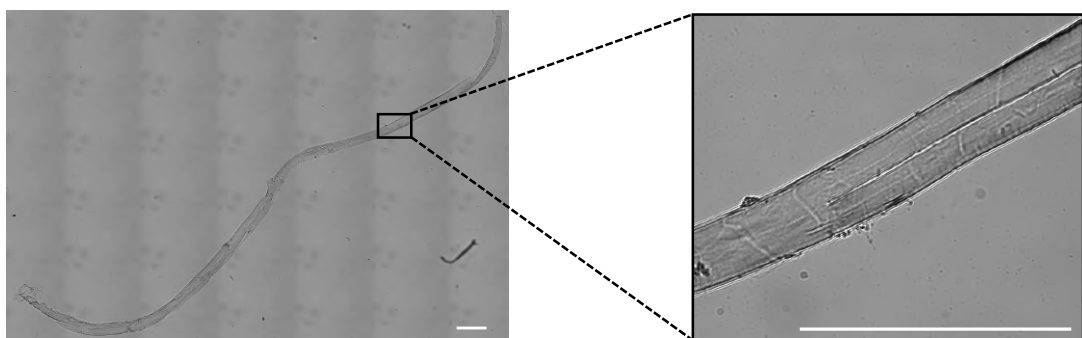
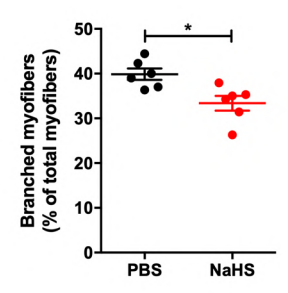


Figure 2

**A****B****C****D****E****F****G**

**Figure 3**

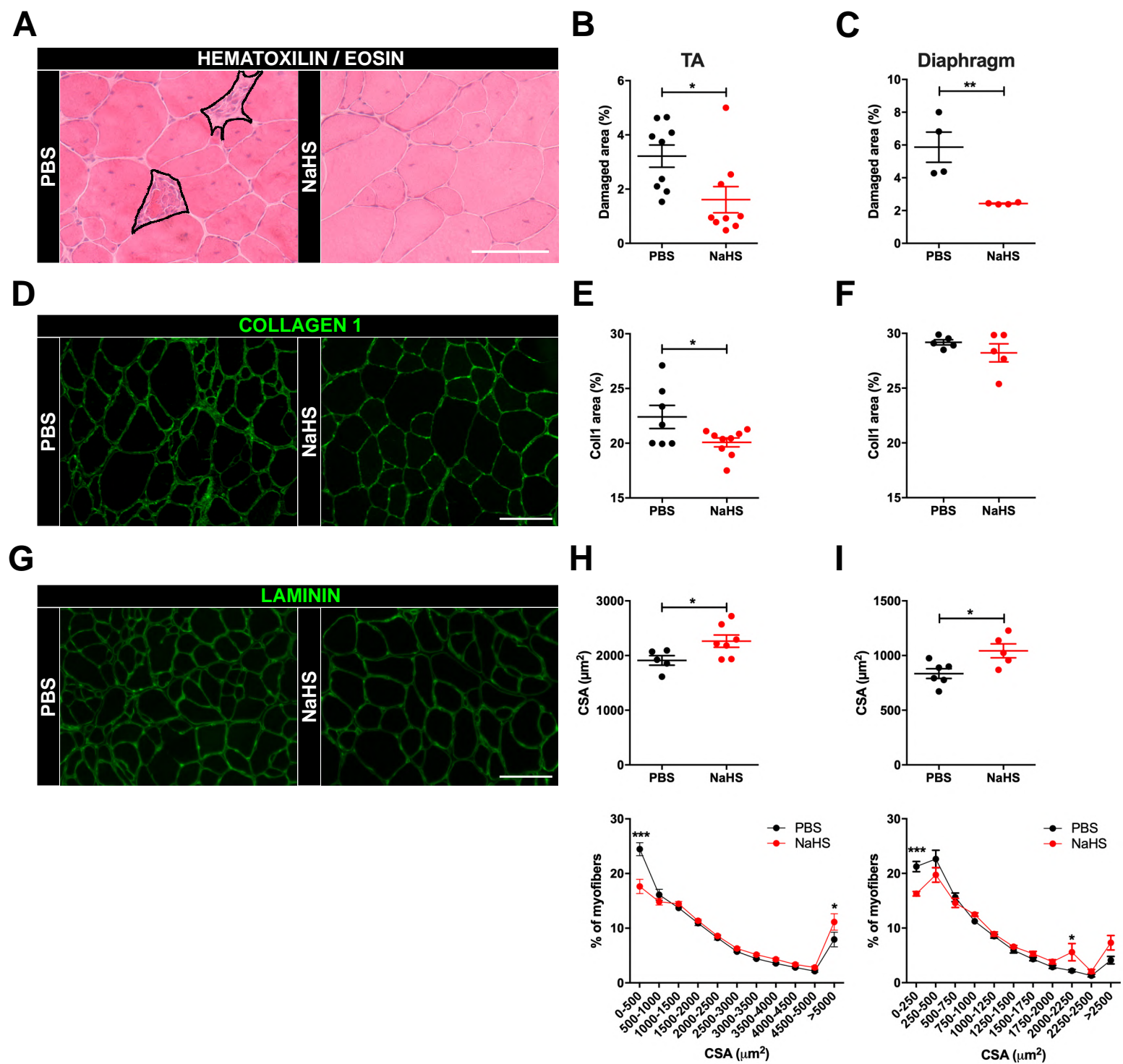


Figure 4

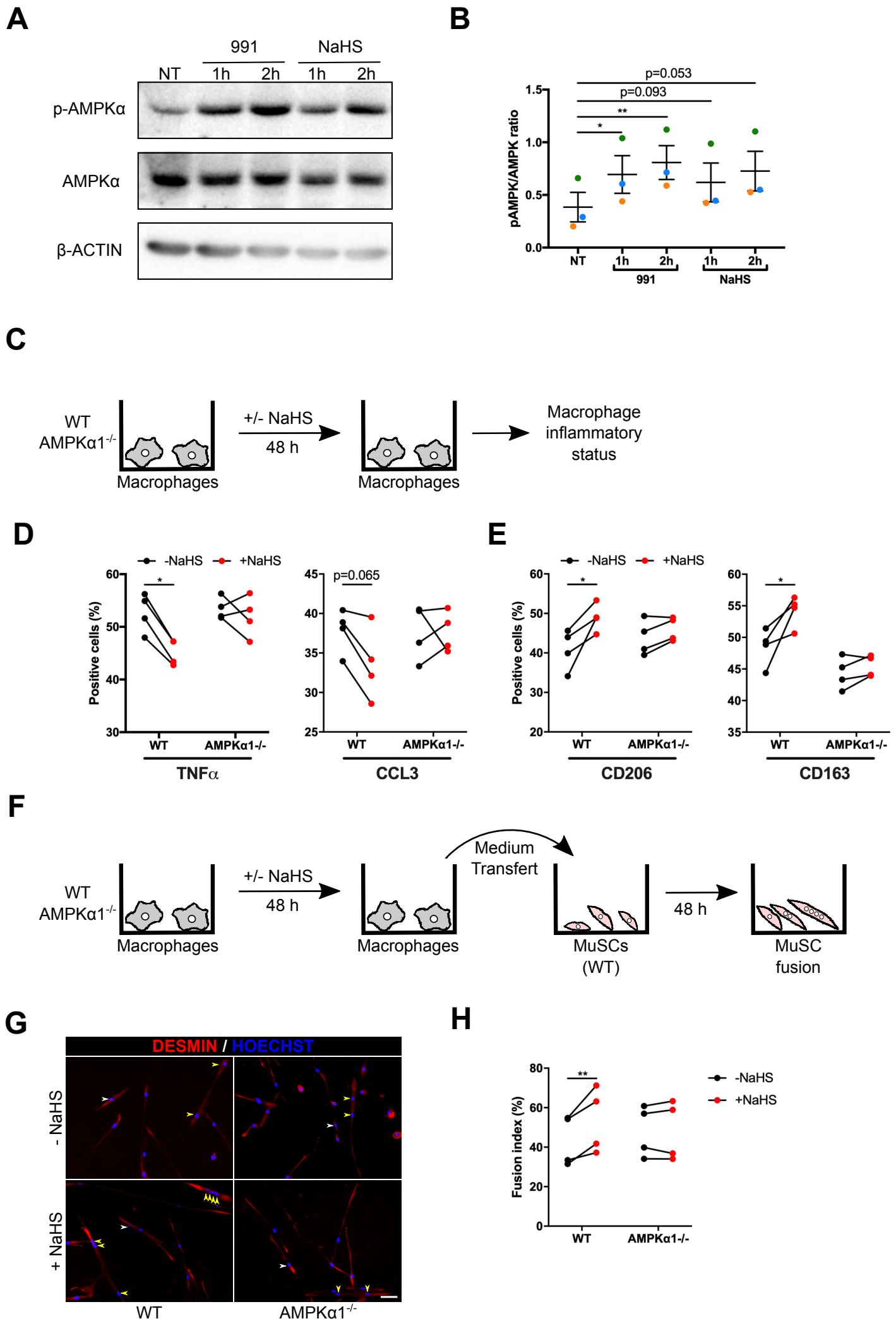


Figure 5

## Supplementary figure legends

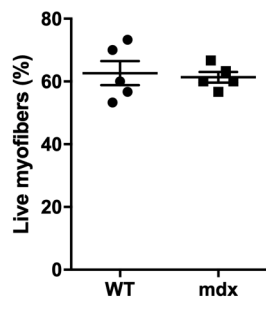
**Figure S1. Viability of isolated myofibers in culture.** BMDMs were cultured with wild-type (WT) or mdx myofibers for 3 days (as described in Fig.1A) and live myofibers (i.e., myofibers that were not hypercontracted) were numerated. Results are means  $\pm$  sem of 5 cultures. Statistical analysis was performed by Student's t test.

**Figure S2. Histological analysis of macrophage inflammatory status in NaHS-treated mdx TA muscle.** Mdx mice were treated daily with PBS or NaHS for 3 weeks (as described in Fig.2A) and TA muscles were harvested. Muscle sections were immunolabeled for F4/80 and pro-inflammatory CCR2 **(A)** or anti-inflammatory CD301 **(B)** markers. The percentage of macrophages positive for the specified marker is shown. Results are means  $\pm$  sem of 8-10 experiments. Statistical analyses were performed by Student's t test.

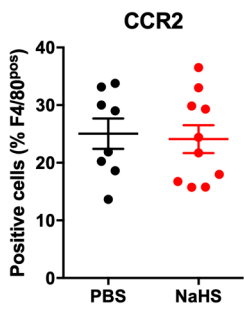
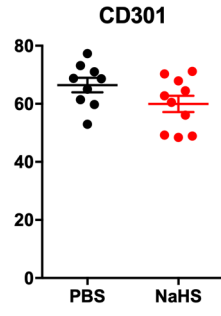
**Figure S3. Histological analysis of myogenic parameters in NaHS-treated mdx TA muscle.** Mdx mice were treated daily with PBS or NaHS for 3 weeks (as described in Fig.2A), TA muscles were harvested and immunostainings were performed. **(A)** Number of satellite cells (as Pax7<sup>pos</sup> cells) normalized per the number of myofibers. **(B)** Newly formed myofibers (as eMHC<sup>pos</sup> myofibers), represented in percent of the total number of myofibers. **(C)** Number of nuclei per myofiber analyzed on a second section of the same muscles shown in Fig3.A-B, located 5 mm apart from the first one. Results are means  $\pm$  sem of 5-6 experiments. Statistical analyses were performed by Student's t test, \*p<0.05.

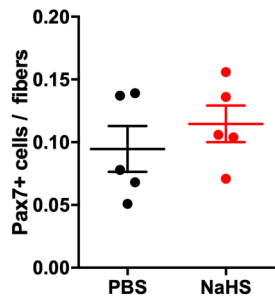
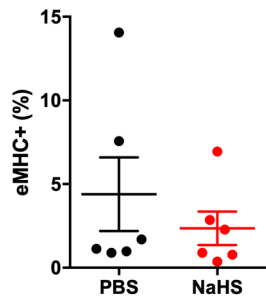
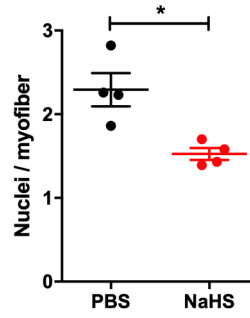
**Figure S4. Histological analysis on a second section level of TA muscle.** Immunolabelings were performed on a second section of the same muscles shown in Fig.4, located 5 mm apart from the first one. **(A)** Percentage of damaged area per muscle section. **(B)** Percentage of Coll1 area. **(C)** Mean CSA (left graph) and repartition of myofibers by size (right graph). Results are means  $\pm$  sem of 4-6 experiments. Statistical analyses were performed by Student's t test

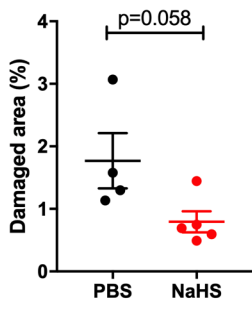
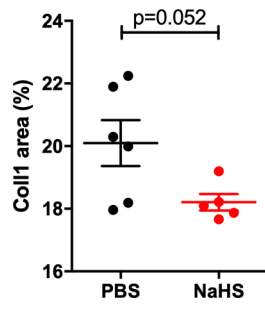
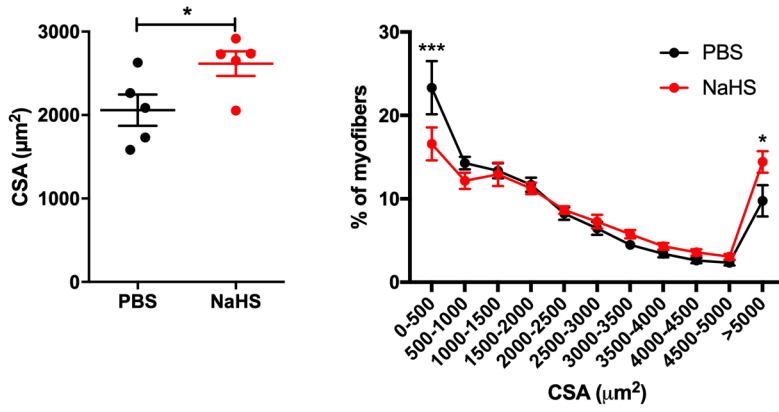
**(A-B and C-left graph)** or two-way ANOVA with multiple comparisons **(C-right graph)**, \* $p < 0.05$ ;  
\*\*\* $p < 0.001$ .



**Figure S1**

**A****B****Figure S2**

**A****B****C****Figure S3**

**A****B****C****Figure S4**